TELKOMNIKA, Vol.17, No.2, April 2019, pp.1047~1054
ISSN: 1693-6930, accredited First Grade by Kemenristekdikti, Decree No: 21/E/KPT/2018
DOI: 10.12928/TELKOMNIKA.v17i2.10533

Influence of input power in Ar/H_2 thermal plasma with silicon powder by numerical simulation

Yulianta Siregar*[1], Yasunori Tanaka[2], Yoshihiko Uesugi[3], Tatsuo Ishijima[4]
[1,2,3,4]Division of Electrical Engineering and Computer Science, Kanazawa University,
Kakuma, Kanazawa 9201192, Japan
[1]Department of Electrical Engineering, University of Sumatera Utara,
Jalan Dr. T. Mansur No.9 Kampus USU, Medan, 20155, telp/fax +6261 8211045, Indonesia
*Corresponding author, e-mail: julianta_srg@yahoo.co.id, julianta@stu.kanazawa-u.ac.jp

Abstract

Numerical simulation in inductively coupled thermal plasma was made on the temperature distribution in argon (Ar)+hydrogen (H_2) induction thermal plasma torch with silicon (Si) powder injection to obtain the temperature distribution and gas flow fields. The ICTP model was used in this research because it has benefit of good repeatability and no contamination process. Interactions between ICTP and injected powder are very complicated to be understood only by related experiments. Influence of input power in ICTP was numerically investigated on thermal plasma temperature fields and powder evaporation. The temperature distributions of thermal plasma and Si vapor distribution were compared at input powers of 20 kW, 30 kW, and 40 kW. Results indicated that higher input power increases the temperature of the thermal plasma with doughnut shape but it slightly enhances evaporation of the powder at the center axis of the plasma torch.

***Keywords**: Ar-H_2, ICTP, input power, numerical simulation, silicon powder injection*

Copyright © 2019 Universitas Ahmad Dahlan. All rights reserved.

1. Introduction

High-power and high-pressure inductively coupled thermal plasma (ICTP) has been widely used for various materials processing such as fabrication of diamond films [1], synthesis of fullerene [2], surface modification of materials, nanomaterial [3, 4], nanocrystallites [5], nanopowder [6, 7] and thermal barrier coatings [8, 9]. Another important in ICTP is influence of input power. The ICTP can be a sufficient heat and chemical source to various materials processing with no contamination. In addition, the ICTP gives one-step direct processing with rapid evaporation of injected raw materials and also rapid cooling of evaporated materials. The rapid cooliing of evaporated material can enhance nucleation of vapor and produce nanoparticles in metastable phase or a non-equilibrium during nanoparticle synthesis with input power by numerical simulation.

During nanoparticle synthesis, feedstock solid power is often supplied into the ICTP to be evaporated. The evaporation rate depends on the temperature distribution and gas flow fields. However, the temperature distribution and gas flow field are also influenced by injected feedstock powder. To understand these complex processes, it is important to model the ICTP with power injection considering its evaporation. Previously, we have developed a numerical model to understand thermal interactions between thermal plasma and particles [10-12]. In this work, we studied the influence of input power on thermal interactions between 99% Ar+1%H_2 ICTP and silicon (Si) feedstock powder injection using our previously developed numerical simulation model [13-16]. Results indicated that influence of input power can increase the thermal plasma temperature in the plasma torch but can just slightly enhance evaporation of feedstock powder at the center axis of the plasma torch.

2. Configuration of Inductively Coupled Thermal Plasma Torch

Figure 1 shows the configuration of the inductively thermal plasma torch used in this numerical simulation. The plasma torch contains two coaxial quartz tubes with 320 mm in length. The inner quartz tube has an internal radius of 35 mm with 3 mm in thickness. An 8

Received July 9, 2018; Revised October 22, 2018; Accepted November 18, 2018

turn-coil is located around the quartz tube to generate the electromagnetic field. The radius of this coil is 58 mm. The generated electromagnetic field forms a thermal plasma inside the torch by inductively coupling. The torch wall of the plasma torch is cooled at room temperature with cooling water. Silicon powder is injected through a water cooled pipe into the ICTP as indicated in Figure 1. The carrier gas is also injected together with the silicon powder through this pipe. For numerical simulation of the ICTP with silicon powder injections, a two-dimensional cylindrical r-z cross section of this plasma torch was set as the calculation space.

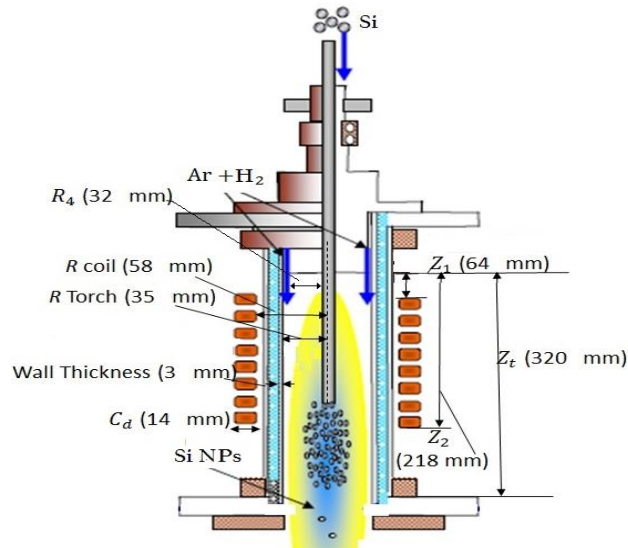

Figure 1. Configuration of ICTP torch

3. Modeling of the Inductively Coupled Thermal Plasma with Powder Injection

3.1. Modelling Assumptions

We have assumed the following conditions for modeling thermal plasma [10-14]; (i) Local thermodynamic equilibrium (LTE) is established in the inductively coupled thermal plasma. Thus, all the temperatures such as the heavy particle temperature, excitation temperature, and electron temperature are identical. In addition, we have equilibrium conditions for all reactions. (ii) The optically thin condition is assumed in the plasma at wavelengths above 200 nm. Whereas at wavelengths below 200 nm, 20% of the total emission coefficient is accounted for as radiation loss to take into consideration the effective light absorption. (iii) Steady, laminar, and axis-symmetric flow is assumed without viscous dissipation. (iv) The particle-particle interactions are neglected for injected particles. (v) The mean free path of plasma components is assumed to be much smaller than the particle radius. (vi) Particle always has spherical shape even at evaporation. (vii) The particles are uniformly heated from the surrounding plasmas. Therefore, evaporation uniformly occurs around the particle surface. (viii) Effects of electronic charging on the particle are not considered. (ix) The rocket effect from ejected evaporation vapor is not taken into account. (x) Silicon feedstock powder particle is evaporated only by heat from the plasma.

3.2. Governing Equation

For an individual feedstock particles supplied through the water-cooled tube, we solve the equation of motion were solved with Lagrangian form considering drag force from the plasma fluid and gravity. In addition, we solve the energy conservation equation of the inidividual particle taking into account heat conduction inside the particle, the heat flux from the plasma and radiation loss from the particle surface. In addition, we considered melting and evaporation process at the surface of the particles. The detail of the calculation can be obtained in reference [12]. Based of the assumptions described above, the thermal plasma is governed by the following equation.

mass conservation:

$$\frac{\partial(\rho u)}{\partial z}+\frac{1}{r}\frac{\partial(r\rho v)}{\partial r}=S_{\mathrm{P}}^{C} \quad (1)$$

momentum conservation.
axial:

$$\rho u\frac{\partial u}{\partial z}+\rho v\frac{1}{r}\frac{\partial u}{\partial r}=\frac{\partial p}{\partial z}+2\frac{\partial}{\partial z}\left(\eta\frac{\partial u}{\partial z}\right)+\frac{1}{r}\frac{\partial}{\partial r}\left[\eta r\left(\frac{\partial u}{\partial z}\right)\right]+\mu_0\sigma\Re\left[\dot{E}_\theta\dot{H}_r^*\right]+S_{\mathrm{p}}^{M_z} \quad (2)$$

radial:

$$\rho u\frac{\partial v}{\partial z}+\rho v\frac{\partial v}{\partial r}=-\frac{\partial p}{\partial z}+\frac{\partial}{\partial z}\left[\eta\left(\frac{\partial v}{\partial z}+\frac{\partial u}{\partial r}\right)\right]+\frac{2}{r}\frac{\partial}{\partial r}\left[\eta r\left(\frac{\partial v}{\partial r}\right)\right]-2\eta\frac{v}{r^2}+\mu_0\sigma\Re\left[\dot{E}_\theta\dot{H}_z^*\right]+S_{\mathrm{p}}^{M_r} \quad (3)$$

swirl:

$$\rho u\frac{\partial w}{\partial z}+\rho v\frac{\partial w}{\partial r}=\frac{\partial}{\partial z}\left(\eta\frac{\partial w}{\partial z}\right)+\frac{1}{r}\frac{\partial}{\partial r}\left[\eta r\left(\frac{\partial w}{\partial r}\right)\right]-\frac{\rho v w}{r}-\frac{w}{r}\frac{\partial r n}{\partial r} \quad (4)$$

energy conservation:

$$\rho u\frac{\partial h}{\partial z}+\rho v\frac{\partial h}{\partial r}=\frac{\partial}{\partial z}\left(\frac{\lambda}{C_{\mathrm{p}}}\frac{\partial h}{\partial z}\right)+\frac{1}{r}\frac{\partial}{\partial r}\left[r\left(\frac{\lambda}{C_{\mathrm{p}}}\frac{\partial h}{\partial r}\right)\right]+\sigma\left|\dot{E}_\theta\right|^2-P_{\mathrm{rad}}-S_{\mathrm{P}}^{E} \quad (5)$$

mass conservation equation for Si vapor:

$$\rho u\frac{\partial Y_{\mathrm{Si}}}{\partial z}+\rho v\frac{\partial Y_{\mathrm{Si}}}{\partial r}=\frac{\partial}{\partial z}\left(\rho D_{\mathrm{Si}}\frac{\partial Y_{\mathrm{Si}}}{\partial z}\right)+\frac{1}{r}\frac{\partial}{\partial r}\left[r\rho D_{\mathrm{Si}}\left(\frac{\partial Y_{\mathrm{Si}}}{\partial r}\right)\right]+S_{\mathrm{P}}^{C} \quad (6)$$

maxwell equation for vector potential :

$$\frac{\partial^2\dot{A}_\theta}{\partial z^2}+\frac{1}{r}\frac{\partial}{\partial r}\left(r\frac{\partial\dot{A}_\theta}{\partial r}\right)-\frac{\dot{A}_\theta}{r^2}=j\mu_0\sigma\omega\dot{A}_\theta \quad (7)$$

$$\dot{H}_z=\frac{1}{\mu_0}\frac{1}{r}\frac{\partial}{\partial r}\left(r\,\dot{A}_\theta\right),\quad \dot{H}_r=\frac{1}{\mu_0}\frac{\partial\dot{A}_\theta}{\partial z} \quad (8)$$

$$\dot{E}_\theta=-j\omega\dot{A}_\theta \quad (9)$$

In these equations, specific heat at constant pressure, mass density, enthalpy, σ: electrical conductivity, p: pressure, η: viscosity, v: radial fow velocity, u: axial fow velocity, r: radial position, z: axial position, ⅄: thermal conductivity, P_rad: radiative loss, Y_Si: mass fraction of Si vapor, D_Si: the effective diffusion coefficient of Si vapor against Ar, μ_0: the permeability of vacuum, A ̇_θ: phasor of the vector potential, ω: the frequency of the coil current, E ̇_θ: phasor of the electric field strength, H ̇_z,H ̇_r: the phasors of axial and radial components of the magnetic field strength, respectively, j: complex factor (j^2=-1). The magnitudes of the phasors including A ̇_θ,E ̇_θ,H ̇_z and H ̇_r are defined as the root mean square values. The asterisks (*) in (11) and (12) indicate the conjugate, and a symbol N is the real part of the phasor. The quantities S_P^C,S_P^(M_z),S_P^(M_r), and S_P^E indicate source terms by the transferred quantities from ablated vapor. These quantities are described later. These terms were computed by PSI cell method developed by P.Proux et al [17-19].

The calculation execution method is the same to our previous work [10-13]. The above governing equations were solved by SIMPLE method after Patankar to obtain gas flow field, and temperature field. Under this calculated field, particle trajectories were calculated by solving motion equation for each indivisual particles, solving particle temperature and size histories along the trajectories. At the same time, the mass, momentum and energy source terms for each control volume from particles were determined. The plasma flow and temprature fields were solved again incorporating these source terms. The new plasma flow field was used to establish new particle trajectories, particle temperature and size history. Iterations are repeated

for as many times as needed convergence of the plasma and the solution that accounts for the mutual interaction of the particle and plasma is finally obtained.

3.3. Calculation Condition

In this calculation, the frequency of the coil current for the ICTP was fixed at 450 kHz. The input power was set to three values of 20 kW, 30 kW, and 40 kW. The pressure was set at 300 Torr (=40 kPa) inside the torch. Total flow rate of Ar and H_2 gas mixture as sheath gas was set to 100 L/min. The fraction of Ar/H_2 was set to 99% Ar-1%H_2. To this ICTP, silicon feedstock powder was assumed to be injected through a water-cooled pipe inserted on the torch axis from the plasma torch head. The injected silicon feedstock powder has a mean diameter of 2 μm and a deviation of 1 μm. The silicon feedstock feed rate was set to 0.5 g/min. The thermodynamic properties of Silicon used in the numerical calculation is summarized in Table 1. In addition, thermodynamic and transport properties of Ar-H_2 mixture and Si vapor were in advance calculated as a function of temperature [20]. Transport properties for the numerical calculationcan was adopted by Chapman-Enskog method [21, 22].

Table 1. Thermodynamic Properties of Silicon Powder

Parameter	Unit	Value
Injection load	g/min	0.5
Mass density	kg/m^3	2329
Melting temperature	K	1687
Boiling temperature	K	2628
Latent heat for melting	J/kg	1787000
Latent heat for evaporation	J/kg	12784000
Specific heat of solid	J/(kg.K)	12
Specific heat of liquid	J/(kg.K)	915
Thermal conductivity	W/(m.K)	150
Emissivity of particle source	(-)	0.3

4. Calculation results

4. 1. The Temperature Distribution of Thermal Plasma

The calculaltion from governing equation in (1) to (9) was made for Si powder injection to 90% Ar-1%H_2 ICTP at input powers of 20 kW, 30 kW, and 40 kW to obtain temperature distirbutions and gas flow pattern of ICTPs, and evaporated mass fraction and also particle size history in Figure 2 to 7. Figure 2(a) shows the temperature distribution of the ICTP with an input power 40 kW, while Figure 2(b) shows the temperature distribution with an input power 30 kW, and Figure 2(c) presents the result at an input power 20 kW. In case of Figure 2(a) with an input power 40 kW, the ICTP has high temperature area about 13000 K in wide region around radial positions of 10 mm<r<26 mm and axial positions 150<z<250 mm. At this high temperature area, the current flows inside the thermal plasma to be heated. On the other hand, as indicated in Figure 2(b), with an input power 30 kW, the high temperature area at temperatures above 13000 K becomes smaller around radial positions of 12 mm<r<24 mm and axial positions of 170 mm <z<240 mm. Furthermore, lower input power 20 kW case as shown in Figure 2(c) presents a further smaller high temperature area at temperatures above 13000 K around radial positions of 16 mm<r<23 mm and axial positions of 205 mm<z<230 mm. This means that increasing input power makes increased temperature in the ICTP. However, as seen along the center axis, the similar temperature around 6000-6500 K can be obtained for 20 kW, 30 kW, and 40 kW. This implies that increasing power just slightly increases the temperature at the center axis of the plasma torch.

To compare the temperature distribution clearly with input powers of 20 kW, 30 kW, and 40 kW in 99% Ar-1%H_2 ICTPs, the radial temperature distributions at axial positions of z=250 mm are plotted in Figure 3. As seen, an increase in input power hardly improves the axial temperature of the ICTP, although the temperatures outside from a radial position of 10 mm rises by increased input power. This implies that evaporatoin of Si feedstock is hardly improved just by increasing input power. On the other hand, Figure 4 shows the axial temperature distribution at radial position of 5 mm, that is at off-axis region, at different three input powers of 20 kW, 30 kW, and 40 kW. At the off-axis region, the temperature recovers faster at higher input power.

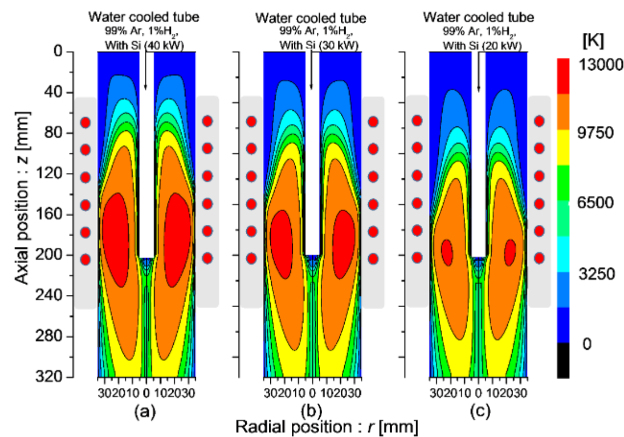

Figure 2. The temperature distribution of 99% Ar-1%H_2 ICTPs with Si powder injection at input powers of 20 kW, 30 kW, and 40 kW

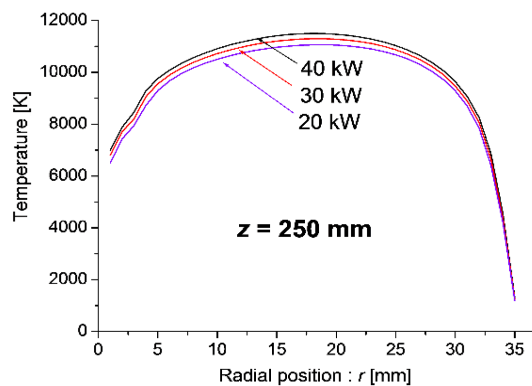

Figure 3. Radial temperature distribution of 99% Ar-1%H_2 ICTP at an axial position of 250 mm with Si powder injection

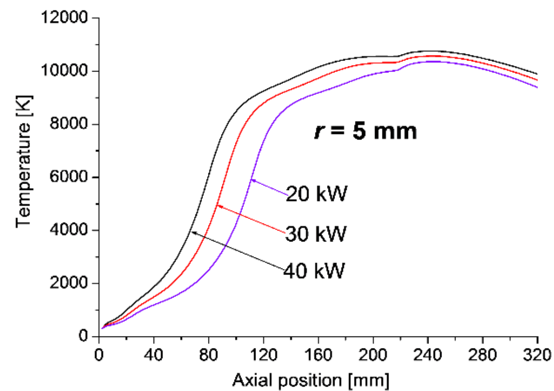

Figure 4. Axial temperature distribution of 99% Ar-1%H_2 ICTP at an radial position of 5 mm with Si powder

4.2. Mass Fraction Distribution of Silicon Vapor

We also consider Si evaporation occurrence in the plasma torch. Figure 5 shows variation in diameters of the 35 particles with 7 different initial diameters injected from 5 different initial positions [23] into the 40 kW-ICTP as a function of axial position. From axial position from 0 to 200 nm, the diameters do not change because all the particles are present inside the water-cooled pipe. From axial position of 200 mm, the particles start flying into the ICTP, and then they are heated. After some fly to be heated, the Si particles have the diameter decreased. This is because of evaproation of the Si particles from the ICTP. In this case, the particles are strongly heated from the ICTP, and then the particle diamater decreases to $1\mu\mathrm{m}$. This evaporation generates Si vapor to the ICTP.

Influence of input power on silicon vapor creation in the ICTP can be seen in Figure 6. As shown in this figure, the mass fraction of Si vapor is distributed far from the tip of the water-cooled pipe where Si feedstock powder is supplied in 99% Ar+1%H_2 ICTPs with 20 kW, 30 kW, and 40 kW. At just below the tip of the pipe, the temperature of the ICTP becomes low because of heat transfer to Si feedstock particle as indicated in Figure 2, and thus the Si feedstock is hardly evaporated. On the other hand, around axial position from 220 mm, Si vapor are generated by evaporation as shown in Figure 5.

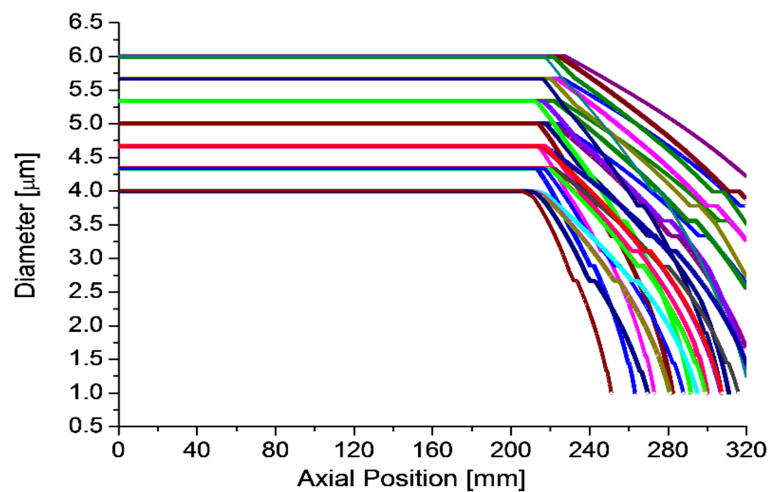

Figure 5. Diameter variation for 35 kinds of Si particles injected with different 7 initial diameters and 5 different initial positions as a function of axial position in 99% Ar-1%H_2 ICTPs

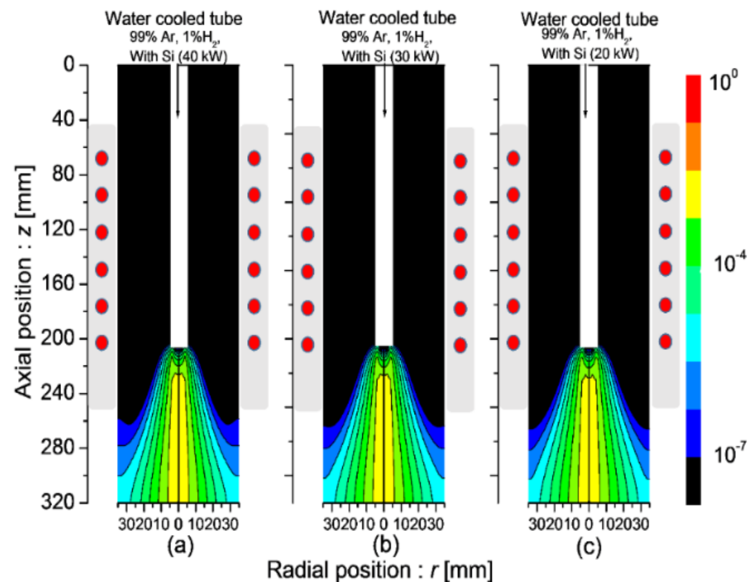

Figure 6. Mass concentration distribution of 99% Ar-1%H_2 ICTPs with Si powder injection at input powers of 20 kW, 30 kW and 40 kW

The evaporation of Si feedstock power causes the contamination of Si vapor inside the ICTP. The contaminated Si vapor is transported by gas flow convection of Ar carrier gas and by diffusion [24, 25]. Thus, silicon vapor is present downstream of the feeding pipe. However, as seen in Figure 6, Si vapor concentration just slightly increase with increasing input power. This implies that just increase in the input power just slightly enhances evaporation rate of Si feedstock powder as long as the feedstock is supplied along the center axis of the torch. This slight increase in evapoartion is because the input power density is essentially low at the center axis in the ICTP.

The injected particle are transported by drag force from the plasma flow and then the plasma flow also transfers evaporated Si material in the torch. Figure 7 presents the streamline inside the ICTP at different input powers of 20 kW,30 kW, and 40 kW. The gas flow field is

almost independent of the input power. Therefore, the injected particle supplied along the plasma torch move around the center axis at which input power density is essentially low.

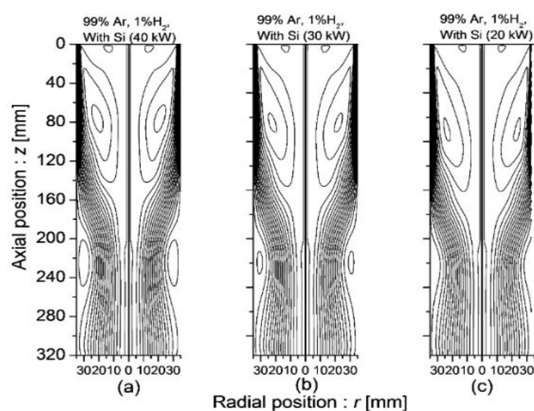

Figure 7. Streamlines in 99% Ar-1%H_2 ICTPs with Si powder injection at input powers of 20 kW, 30 kW, and 40 kW

5. Conclusion

This research investigated the influence of input power on the temperature distribution in argon (Ar) and hydrogen (H_2) induction thermal plasma with silicon (Si) powder injection. The calculated temperature distributions of 99%Ar-1%H_2 thermal plasma and Si powder injection were compared with different input powers of 20 kW, 30 kW, and 40 kW. Results indicated that higher input power increases the temperature of the thermal plasma but it slightly enhances evaporation of the powder at the center axis of the plasma torch.

This numerical calculation research was made to obtain temperature field and gas flow field and evaporated mass fraction from very complicated interactions between thermal plasma and particle injection, which cannot be understood only by experiments. The calculated temperature distributions of 99% Ar-1%H_2 thermal plasma and Si powder injection were compared with different input powers of 20 kW, 30 kW, and 40 kW. Results indicated that higher input power increases the temperature of the thermal plasma with doughnut shape but it slightly enhances evaporation of the powder at the center axis of the plasma torch.

Acknowledgment

The authors thank to Kanazawa University, Japan and Ministry of Research, Technology and Higher education (KEMRISTEKDIKTI) of Indonesian Government for the existing bilateral academic-cooperation. An appreciation is also granted to Indonesia Endowment Fund for Education (LPDP) that provides fund through a BUDI-LN Scholarship Scheme.

References

[1] S Gottlieb, N Wohrl, S Schulz, V Buck. Simultaneous synthesis of nanodiamonds and graphene via plasma enhanced chemical vapor deposition (MW PE-CVD) on copper. *SpringerPlus*. 2016; 5: 568.

[2] KS Kim, A Moradian, J Mostaghimi, G Soucy. Modeling of induction plasma process for fullerene synthesis: Effect of plasma gas composition and operating pressure. *Plasma Chem and Plasma Process*. 2010; 30: 91-110.

[3] P-J Chu, S-Y Wu, K-C Chen, J-L He, A. Yerokhin, A. Matthews. Nano-structured TiO2 films by plasma electrolytic oxidation combined with chemical and thermal post-treatments of titanium, for dye-sensitised solar cell applications. *Thin Solid Films*. 2010; 519: 1723-1728.

[4] Shigeta, *Numerical investigation of nano-material processing by thermal plasma flows*. Proceedings of the Joint Workshop on High Performance Computing on Vector Systems, and Workshop on Sustained Simulation Performance. Sendai, 2013; 169-182.

[5] Ishigaki T, Li J G. Synthesis of functional nanocrystallites through reactive thermal plasma processing. *Sci. Technol. Adv. Mater*. 2007; 8: 617–23.
[6] Tong L, Reddy RG. Thermal plasma synthesis of SiC nano-powders/nano-fibers. *Mater. Res. Bull*. 2006; 41: 2303–10.
[7] Shigeta M, Watanabe T, Nishiyama H. Numerical investigation for nano-particle synthesis in an RFinductively coupled plasma. *Thin Solid Films*. 2004; 457: 192–200.
[8] J. Mao, M. Liu, C.G. Deng, C.M. Deng, K.S. Zhou, Z.Q. Deng. Preparation and distribution analysis of thermal barrier coatings deposited on multiple vanes by plasma spray-physical vapor deposition technology. *J.Eng. Mater. Technol*. 2017; 139041003.
[9] Mao WG, Chen YY, Wang YJ, Zhou M, Yang HY, Wang Z, Dai CY, Chen X, Fang DN. A multilayer structure shear lag model applied in the tensile fracture characteristics of supersonic plasma sprayed thermal barrier coating systems based on digital image correlation. *Elsivier, Surface and Technology*. 2108; 350: 211-226.
[10] C Wang, Y Tanaka, T Sakuta. Modeling of Ar Induction Thermal Plasma with an Injection of PTFE Powder. *Trans. IEEJ.* 2004;124-PE: 440-46.
[11] Y Takeuchi, Y Tanaka, Y Uesugi, S Kaneko, S Okabe. Numerical simulation of thermal interaction between polymer and Ar induction thermal plasma. *Trans. IEEJ.* 2007; 127-PE: 739-46.
[12] Y Tanaka, Y Takeuchi, Y Uesugi, S Kaneko, S Okabe. Numerical and experimental investigations on thermal interaction between thermal plasma and solid polymer poeders using induction thermal plasma technique. *J. Phys. D: Appl. Phys*. 2008; 41: 025203.
[13] Y Tanaka, T Sakuta. Investigation of plasma quenching efficiency of various gases using induction thermal plasma technique: effect of various gas injection on Ar thermal ICP. *J. Phys. D: Appl. Phys* 2002; 2149-58.
[14] Y Siregar, N Kodama, Y Tanaka, T Ishijima, Y Uesugi. Numerical simulation on thermal plasma temperature field in torch for different conditions. *IOP Conference Series: Materials Science and Engineering*. 2018; 309(1): 012090.
[15] Guo QJ, Ni GH, Li Li, Lin QF, Zhao YJ, Sui SY, Xie HB, Duan WX, Meng YD. Effects of input power, gas flow rate and hydrogen concentration on Cu film deposition by a radio frequency driven non-thermal atmospheric pressure plasma jet. Elsevier, Thin Solid Films. 2018; 660: 493-498.
[16] V Colombo, E Ghedini, M Gherardi, P Sanibondi. Evaluation of precursor evaporation in Si nanoparticle synthesis by inductively coupled thermal plasmas. IOP Publishing. 2013; 22: 035010
[17] P Proulx, J Mostaghimi, MI Boulos. Plasma particle interaction effects in induction plasma modeling under dense loading conditions. *Int. J. Heat Mass Transfer*. 1985; 28:1327-36.
[18] P Proulx, J Mostaghimi, MI Boulos. Heating of powder in an r.f. inductively coupled plasma under dense loading conditions. *Plasma Chem. Plasma Process*. 1987; 7: 29-52.
[19] J Mostaghimi, P Proulx, MI Boulos. An analysis of the computer modeling of the flow and temperature fields in an inductively coupled plasma. *Numerical Heat Transfer*, 1985; 8: 187-201.
[20] JM Yos. Transport properties of nitrogen, hydrogen, oxygen and air to 30 000 K, *AVCO Technical Memoandum RAD-TM*. 1963; 63-7.
[21] S Chapman, TG Cowling. The Mathematical Theory of Non-Uniform Gases Third Edition. *Cambridge University Press*.1970.
[22] RS Devoto. Transport coefficients of partially ionized argon. *Phys. Fluid*. 1967 ; 10. 354-64.
[23] Li J G, Ikeda M, Ye R, Moriyoshi Y, Ishigaki T. Control of particle size and phase formation of TiO2 nanoparticles synthesized in RF induction plasma. *J. Phys. D: Appl. Phys*. 2007; 40: 2348–53.
[24] Devoto RS. Transport coefficients of partially ionized argon. *Phys. Fluid*. 1967; 10: 354–64
[25] Mengyao Wei, Bin He, Qian Liang, Sivanand Somasundaram, Chuan Seng thang, Evelyn N. Wang. Optimization and thermal characterization of uniform silicon micropillar based evaporators. *Elsevier, International Journal of Heat and Mass Transfer.* 2018; 127: 51-60.